Competing active and passive interactions drive amoebalike crystallites and ordered bands in active colloids

Abraham Mauleon-Amieva,[1,2,3,4] Majid Mosayebi,[5,6] James E. Hallett,[1,2,3] Francesco Turci,[1] Tanniemola B. Liverpool,[5,6] Jeroen S. van Duijneveldt,[2] and C. Patrick Royall [1,2,3]

[1]*H.H. Wills Physics Laboratory, Tyndall Avenue, Bristol BS8 1TL, United Kingdom*
[2]*School of Chemistry, University of Bristol, Cantock's Close, Bristol BS8 1TS, United Kingdom*
[3]*Centre for Nanoscience and Quantum Information, Tyndall Avenue, Bristol BS8 1FD, United Kingdom*
[4]*Bristol Centre for Functional Nanomaterials, Tyndall Avenue, Bristol BS8 1FD, United Kingdom*
[5]*School of Mathematics, University of Bristol, Bristol BS8 1TW, United Kingdom*
[6]*BrisSynBio, Life Sciences Building, Tyndall Avenue, Bristol BS8 1TQ, United Kingdom*

Swimmers and self-propelled particles are physical models for the collective behavior and motility of a wide variety of living systems, such as bacteria colonies, bird flocks, and fish schools. Such artificial active materials are amenable to physical models which reveal the microscopic mechanisms underlying the collective behavior. Here we study colloids in a dc electric field. Our quasi-two-dimensional system of electrically driven particles exhibits a rich and exotic phase behavior exhibiting passive crystallites, motile crystallites, an active gas, and banding. Amongst these are two mesophases, reminiscent of systems with competing interactions. At low field strengths activity *suppresses* demixing, leading to motile crystallites. Meanwhile, at high field strengths, activity *drives* partial demixing to traveling bands. We parametrize a particulate simulation model which reproduces the experimentally observed phases.

I. INTRODUCTION

From living organisms to synthetic colloidal particles, active systems display exotic phenomena not attainable by matter at thermal equilibrium [1–12], such as swarming [13,14], cluster formation [15–18], phase separation in the absence of attractions [6,19–22], banding [23], and unusual crystallization behavior [24]. This is due to continuous energy consumption which occurs in a wide range of systems which can result in collective behavior at very different length scales, from the cell cytoskeleton [25,26], tissues [27], and bacterial colonies [28–31] to larger scales such as insect swarms [32], fish schools [33], and bird flocks [34]. Artificial active materials, composed of microswimmers, active colloids or vibrating granular particles [7,15,24,29,35], or even synthetically modified living systems such as bacteria [21,36], provide a suitable testing ground where the behavior of active matter may be carefully probed to extract the new physical principles of this class of matter.

While some progress has been made in the context of mapping to equilibrium behavior [6,19,37–40], with notable exceptions [6,41–43], theoretical approaches remain less developed. Key to the development of a theoretical understanding is to use simple models of active particles. While these capture some of the complex behavior observed experimentally, for example, collective motion and demixing [6,41,44–52], the link between experiment and theory in active matter is often rather qualitative. As a result, a comprehensive understanding of how and which microscopic mechanisms lead to the emergence of complex structures in experimental active systems remains elusive. Here, we use particle-resolved studies to observe the Quincke roller system, active colloids which exhibit swarming and flocking. We parametrize our experimental system at the microscopic level of the interacting particles [53,54]. While intriguing boundary phenomena are observed in this system [55], here we focus on bulk phase behavior.

At low-to-moderate motility, we reveal the importance of competing passive interactions (long-ranged attractions) driving crystallization and activity which leads to meltinglike and evaporationlike behavior. At high motility, the role of passive and active interactions is *reversed*: Activity drives demixing resulting in a banding phase, whose ordered local structures result from the repulsive core of the particles. This competition between passive and active interactions is reminiscent of well-known passive systems with competing interactions such as amphiphiles, block copolymers, and mixtures of charged colloids and nonabsorbing polymer where competing interactions lead to modulated phases such as clusters and lamellae [56–59], which indeed resemble some structures we find here and which have been shown to persist in active systems [17,41]. Our approach shows how one may use bottom-up designs of particulate active matter with precisely controllable macroscopic behavior.

In the system we study, the application of a uniform dc electric field above a critical field strength E_Q induces *Quincke rotation* of colloidal particles, which leads to directed motion by coupling their translation and diffusion near a surface
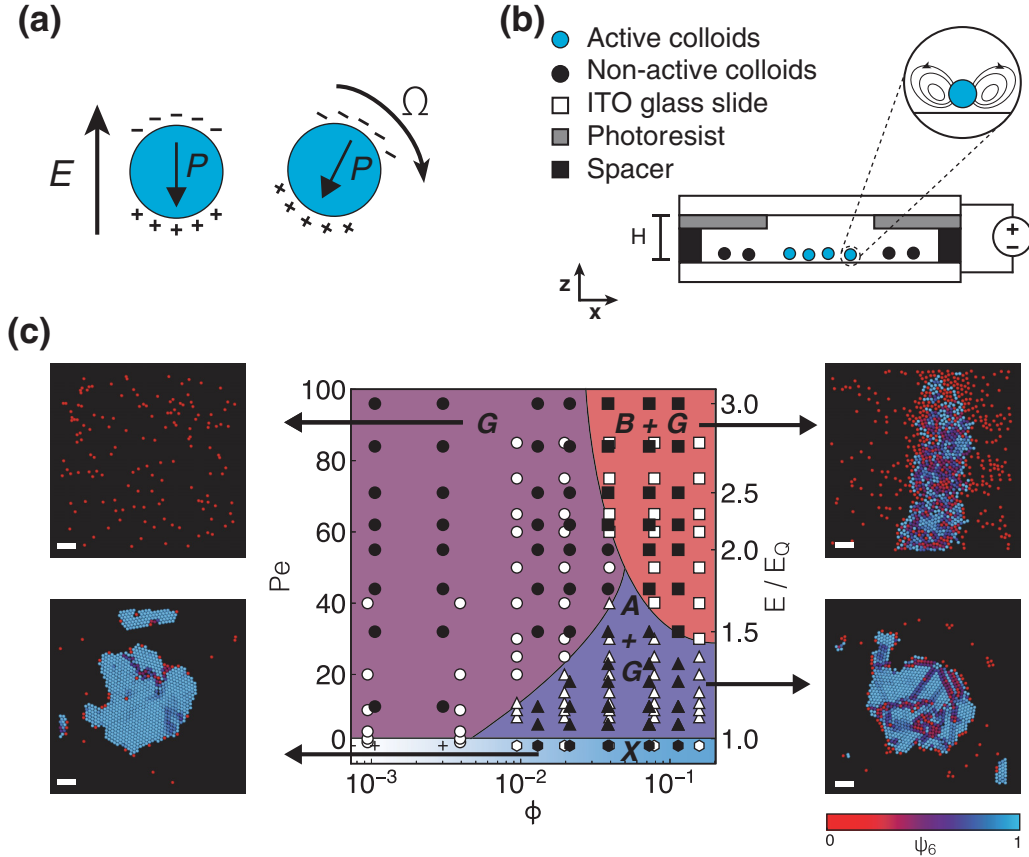
FIG. 1. Phase diagram of Quincke rollers as a function of activity. (a) Schematic representation of mechanism of Quincke rolling. The charge distribution around the sphere forms a dipole oriented inversely to the field direction, and any fluctuation in the dipole orientation leads to particle rotation with a constant angular speed Ω. The field-dependent activity is translated to the Péclet number, as described in the text. (b) Experimental setup. Colloidal particles are suspended within a sample cell made of conductive glass slides. Colloids are confined by an electrokinetic flow to the region of interest and they become active (blue particles). The induced electrohydrodynamic flow is represented by the solid lines in the amplified illustration. This flow field leads to long-ranged electrohydrodynamic interactions between the particles [72]. (c) Phase behavior in the area fraction: Péclet number plane. In the low activity regime, electrohydrodynamic interactions due to flow fields [see inset in (b)] result in (passive) crystallite formation at sufficient area fraction. On increasing the activity, e.g., Pe = 2 ($E = E_Q$, with $E_Q \approx 8 \times 10^5$ Vm^{-1}), the particles self-propel sufficiently that the dynamics change markedly [see Supplemental Material, Fig. S2(b) and Movie 1 [67]], and the active crystals split and coalesce with one another. With a further increase of activity, the crystallites melt and we find polar bands propagating through active gas. Black and white symbols represent experimental and numerical data, respectively. Symbols: ○ represent passive crystals (X), ◎ active gas (G), △ active crystals and gas (A+G), □ bands and gas (B+G). Solid lines are drawn guides. Experimental snapshots for every phase in the diagram are indicated by arrows. Particles are colored according to their hexagonal order parameter ψ_6, whose magnitude is indicated by the color bar. Scale bars represent 10 μm.

[53,60]. In the absence of a field, the particles behave as conventional passive Brownian colloids. At low field strengths, while remaining nonmotile, particles agglomerate into crystals due to to long-ranged attractive interactions which arise from electro-osmotic flows [Fig. 1(a)] [61–63]. Above E_Q, the particles undergo Quincke rotation [64–66] and become motile [Fig. 1(b)] so that the electro-osmotically generated crystallites transition into a highly mobile active state reminiscent of amoebae (see Supplemental Material, Movies 1–3 [67]).

Unlike "living crystals" [16], and systems exhibiting motility-induced phase separation [6,18,20,21], here the aggregation is driven by long-ranged electrohydrodynamic interactions [61–63]. These "amoebae" are motile and characterized by a highly dynamic outer surface, and dissolve into an isotropic active gas as we increase the field strength. Finally, at very high field strengths we find that the system transitions to a inhomogeneous polar state ("banding") that has previously been investigated numerically and analytically in active matter systems [23,44,68–70], and experimentally observed [53,71], but here we find a significant degree of local ordering. We investigate the rich structural and dynamical properties of our system using a range of static and dynamic order parameters.

Central to our approach is to capture, quantitatively, the behavior of the experimental system with a simulation model which captures the essentials of the system [53]. In this way, we provide the means to predict the behavior of active matter systems in a rather accurate fashion.

II. METHODOLOGY

A. Experiments

A more extensive description of the experimental setup shown schematically in Fig. 1(b) is included in the Appendix. We use the so-called Quincke electrorotation mechanism of colloidal rollers [53]. A uniform electric field E is applied to the suspension. Above a critical field strength E_Q, the symmetry of the electric charge distribution at the colloid surface breaks spontaneously. As a result, an electric torque acting on the colloids leads to rotation with a constant rate around a random axis transverse to the field E [Fig. 1(a)] [64,65]. Upon sedimentation, a quasi-two-dimensional (quasi-2D) system forms, and rotation couples with translation. As a result, roller motion along a random direction is observed.

We use suspensions of colloidal particles of diameter $\sigma = 2.92$ μm in a nonaqueous ionic solution. Experiments are performed using sample cells made of two indium-tin-oxide (ITO) coated glass slides separated by double-sided tape. The ITO layers are used for the application of the electric field in the z direction. Simultaneously, rollers are confined within a square region with the application of the field. This region is created by the removal of a photoresist layer, as illustrated in Fig. 1(b). Note that a nonzero current develops solely within the square region of the cell. With Quincke rotation acting on the system, the roller trajectories are restrained to the confinement region. We translate the resultant field-dependent motion to dimensionless Péclet numbers Pe, which characterize the strength of the active motion with respect to the thermal diffusive (colloidal) motion. We henceforth characterize the static and dynamic behavior of the system with increasing area fractions ϕ and field strengths. Throughout, we use the Brownian time for a colloid to diffuse its own radius in 2D, $\tau = \sigma^2/D_t \approx 9$ s, as the unit of time, where D_t is the translational diffusion constant.

B. Simulations

The Quincke rollers are subject to forces and torques due to excluded volume repulsions, as well as self-propulsion, alignment, and attractions generated by the electrohydrodynamic interactions of the particles with their environment and each other [53,72]. They can be modeled as *active Brownian particles* with an additional *active aligning torque*, whose active and passive forces and torques can be quantitatively specified. We implement Brownian dynamics simulations, with the following equations of motion for positions and orientations $\mathbf{r}_i, \theta_i$:

$$\dot{\mathbf{r}}_i = \frac{D_t}{k_B T}[\mathbf{F}_i + f^p \hat{\mathbf{P}}_i] + \sqrt{2D_t}\xi_i^t, \tag{1}$$

$$\dot{\theta}_i = \frac{D_r}{k_B T}\mathcal{T}_i + \sqrt{2D_r}\xi_i^r, \tag{2}$$

where $\mathbf{F}_i$ is the interparticle force on the ith roller, f^p is the magnitude of the active force, $\hat{\mathbf{P}}_i = (\cos\theta_i, \sin\theta_i)$ is the direction of motion of the ith roller, $\mathcal{T}_i$ is the torque on the ith roller which incorporates alignment terms, and $\xi_i^{t,r}$ is a Gaussian white noise of zero mean and unit variance. D_r is the rotational diffusion constant. The direct interactions $\mathbf{F}_i$ include a "hard"-core and long-range attraction, the latter to

model the electrohydrodynamic contribution. This pertains to long-ranged hydrodynamic attractions induced by solvent flow [61–63]. Further details of the model (which is partly based on Ref. [53]) and the simulation parameters, and the procedure by which the parameters were mapped to the experiment may be found in the Appendix. We emphasize that we use *one* set of interaction parameters to describe the simulations, that is to say, we only vary the area fraction and Péclet for all the state points studied.

C. Determining the Péclet number

Before moving to the discussion of our results, we first describe our mapping of field strength to Péclet number between experiment and simulation. We obtain the bare translational diffusion coefficient of the passive system D_t measured at equilibrium. Particle velocity v and the characteristic timescale for the rotational diffusion $\tau_r = D_r^{-1}$ for a dilute sample with area fraction $\phi \approx 0.001$ are obtained from the fitting to the mean square displacement (MSD) of active particles in the dilute (gas) regime,

$$\langle \Delta r^2(t) \rangle = 4D_t t + \frac{v^2 \tau_r^2}{3}\left[\frac{2t}{\tau_r} + \exp\left(\frac{-2t}{\tau_r}\right) - 1\right]. \tag{3}$$

To extract the parameters of Eq. (3) from the experiments we consider a series of similarly dilute samples at different field strengths. We estimate the dimensionless Péclet number as $\text{Pe} = 3v\tau_r/\sigma$, for each measured velocity in the different states obtained in the experiment. The Péclet number is defined in terms of Quincke rotation. However, since this is related to the threshold field strength E_Q where Quincke rotation is initiated, we find that for low field strengths, Pe is small and only weakly dependent on the field $E \ll E_Q$, Pe ~ 0. Once the particles become motile, for our system the two appear to coupled for $E > E_Q$, as Pe scales with $[(E/E_Q)^2 - 1]^{1/2}$, (see Fig. S1 in the Supplemental Material [67]). Note that because the particles are colloidal, they can only be quasi-2D, and we expect slip boundary conditions between the particles and the substrate.

III. RESULTS

We now present our main findings. First, we consider the phase behavior of the system as a function of the activity, represented by the Péclet number which we obtain from measuring particle mobility, and as a function of area fraction. At zero field strength (Pe $= 0$), we obtain Brownian hard disks which form a 2D colloidal fluid for the area fractions we consider. Upon increasing the field strength for $\phi \gtrsim 0.03$, the system exhibits a novel phase behavior owing to a coupling between nonequilibrium electrohydrodynamic interactions due to solvent flow and electrically induced activity (Quincke rotation). Then, by the use of a variety of dynamic and static order parameters, we identify the nature of the transitions between these states.

A. Crystallization

At sufficient area fraction, we find that particle condensation to form crystallites emerges at low field strength, e.g.,

Pe ≈ 0 ($E < E_Q$). This is due to the long-ranged electrohydrodynamic interactions [Fig. 1(b)] [72]. In our experiments, colloids act as dielectric regions perturbing the electric charge distribution, therefore inducing a flow of ions with a component tangential to the substrate [72]. In the vicinity of such an electro-osmotic flow, the particles experience transverse motion leading to the formation of crystallites [Fig. 1(b)]. We find crystallization for area fractions $\phi \gtrsim 10^{-2}$. We emphasize that this may be due to the finite size of our experimental cells. That is to say, even the passive system is likely out of equilibrium and for sufficient waiting time, we expect crystallite formation for $\phi \lesssim 10^{-2}$.

B. Activity-induced phase transitions

Upon increasing the field strength, we can exploit the Quincke mechanism that triggers spontaneous rotation [Fig. 1(a)] to study the behavior of self-propelled rollers. For this to occur, the viscous torque acting on the particle must be overcome, hence the field needs to be sufficient to initiate rolling ($E \geqslant E_Q$). When increasing the activity above Pe ≈ 2 ($E = E_Q$), we observe crystallite motility, that is to say, the crystallites are mobile by themselves (see Supplemental Material, Movie 1 [67]), related to clustering behavior in Quincke rollers modified to exhibit run-and-tumble behavior [73]. These active crystallites arise from the interplay of electrohydrodynamic interactions [61,72] and the Quincke electrorotation of the rollers. Note that for our system, the aggregation resulting from passive interactions does not fully suppress motility, as recently suggested for high-density active solids [55].

We further find coalescence and splitting of the crystallites, yet the local hexagonal symmetry remains, as can be seen in certain bacteria colonies [31] and chiral swimmers [74]. We term this an "amoeba phase" since the motility leads the aggregate to constantly reshape in a fashion reminiscent of the motion of amoebae, as shown by the time sequence in Fig. S2(b) (also see Supplemental Material, Movie 1 [67]). These amoebae appear to be in a nonequilibrium steady state. However, such an inhomogeneous state is reminiscent of mesophases in passive systems, but here activity suppresses demixing, playing the role of long-ranged repulsion in so-called "mermaid" systems [57–59,75] and consistent with some recent predictions of active liquids [41]. We note that, for this emergence of motility, E is substantially larger than E_Q. There may be some suppression of the transition to Quincke rotation by the dense packing in the crystallites, but we caution that E_Q is approximate in any case.

On further increasing the field to $E = 1.75E_Q$ (Pe $= 44$), with $\phi \leqslant 4 \times 10^{-2}$ Quincke rotation triggers breakdown of the active crystallites into an "active gas" of colloidal rollers undergoing displacement in random directions [Fig. 1(c)]. Previously, it was shown experimentally that the increase in area fraction results in homogeneous polar phases and vortices [53,54]. Here, we note that the onset to polar collective motion occurs experimentally with area fraction $\phi = 4 \times 10^{-2}$ and Pe $\geqslant 63$. Further increase in area fraction results in traveling bands through the gas at lower activity values, i.e., Pe ≈ 32.

These bands form perpendicular to the direction of particle motion (which self-organizes into a strongly preferred direction) (see Supplemental Material, Movies 4 and 5 [67]). This is related to banding observed in earlier experiments with Quincke rollers [53], but here the area fraction in the band is very much higher, leading to local hexagonal order [see Fig. 1(c)].

The traveling bands are akin to the liquid fractions in flocking models [70,76], but here the high local area fraction leads to hexagonal order in the bands. However, within the activity and density values measured no homogeneous phase develops as in earlier experiments with Quincke rollers [53]. In our simulations, we see one band in the box. We leave the analysis of whether this is activity-driven microphase separation, or full demixing for a later finite-size scaling analysis. This local hexagonal order within the bands contrasts with the unstructured bands seen in the Vicsek model [23]. Here, it is the activity which *drives* the banding, i.e., particle demixing. This is quite unlike the case of the amoebae above, where activity *suppresses* full demixing.

C. Local structure

Having qualitatively introduced the behavior we encounter in our system in Fig. 1, we now proceed to consider the phase transitions in more detail. In order to determine the nature of the transitions we require suitable order parameters. We first consider the structural properties of the phases we encounter: Passive fluid, passive crystal, active crystallite ("amoebae"), active gas, and bands. Given the richness of the phase behavior, it is unlikely that one single order parameter will prove sufficient, and we find this to be the case. We begin with the 2D bond-orientational order parameter $\psi_6 = (1/N) \sum_{i=1}^{N} |\psi_6^i|$. Perfect hexagonal ordering is indicated by $\psi_6 = 1$, whereas a completely disordered configuration gives $\psi_6 = 0$. See Appendix, Sec. 3, for more details of ψ_6.

In Fig. 2(a), we plot the average ψ_6 as a function of Pe and the applied electric field for both experiment and simulation. We emphasize that, given the simplicity of our model, and of our mapping, the agreement between experiment and simulation is remarkable. We find low ordering of the passive Brownian system (at $E = 0$ or Pe $= 0$). With a slight increase in the field strength to $E < E_Q$, we observe a rapid rise in ψ_6 to ≈ 0.9 that corresponds to the crystallization transition driven by the electrohydrodynamic interactions. In this regime, the system is composed of many crystallites that barely move. It is possible that there may be a condensed liquid (or hexatic) phase [77], although this is not apparent in our data, and the transition appears first order within the field strengths we have sampled. We believe this to be similar to equilibrium 2D attractive systems undergoing crystallization and move on to consider the activity-driven transitions.

Increasing the activity further into the amoeba phase, ψ_6 starts to decrease. However, ψ_6 remains significantly above zero indicating the amoeba clusters are crystal-like. While this state is far from equilibrium, the ψ_6 value exhibits temporal fluctuations consistent with a steady state [Supplemental Material, Fig. S2(a) [67]] and local order parameter ψ_6 reveals rotational motion of the ameobae. We infer that to distinguish the (passive) crystallites from the amoebae, some kind of dynamic order parameter may prove suitable, and return to this below. At larger Pe ($11 \lesssim$ Pe $\lesssim 40$), the value of ψ_6,
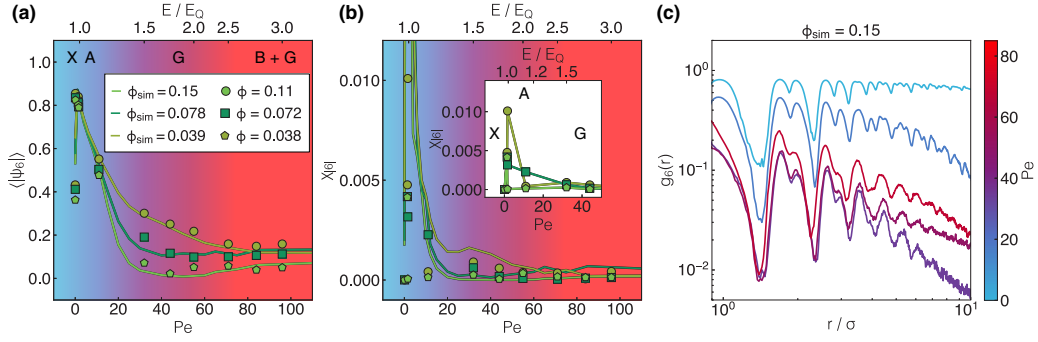
FIG. 2. Changes in local structure as a function of field strength for Quincke rollers. (a) Local order determined with the bond-orientational parameter ψ_6 upon increasing Pe values. (b) Fluctuations of the bond-orientational parameter χ_6 as defined in the text. Inset displays experimental measurements where a peak develops at the transition between the crystallites and the amoeba phase. Symbols and lines in (a) represent experimental and numerical data respectively for both (a) and (b). (c) Orientational correlation functions $g_6(r)$ for Pe as indicated in the color bar. Data obtained from simulations with $\phi = 0.15$. In (a) and (b) and in subsequent figures, the phases are denoted as X (crystallites), A (amoebae), B + G [(active) gas and banding].

drops markedly, as the amoebae "dissolve," apparently in a continuous fashion. Finally, at very high Pe (Pe $\gtrsim 40$), we see the emergence of banding, a form of phase separation driven by activity. The value of ψ_6 again shows signs of increase for $\phi < 0.16$.

To gain further insight into these transitions, in Fig. 2(b) we plot the fluctuations in the hexatic bond-orientation order parameter which we take as $\chi_6 = \langle \psi_6^2 \rangle - \langle \psi_6 \rangle^2$ where the average is over different snapshots. Further details are provided in the Appendix, Sec. 3. At low Péclet numbers, we see good agreement between the experiment and simulation, but when the motility is higher, the simulations decay toward the active gas faster than the experiments. However, we find no enhancement in χ_6 around the amoeba-gas phase boundaries, indicating that the transition is a crossover rather than a first-order-like transition between different phases.

To quantify the spatial correlations in ψ_6, in Fig. 2(c), we plot $g_6(r)$ defined as

$$g_6(r = |\mathbf{r}_i - \mathbf{r}_j|) = \langle \psi_6^{i*} \psi_6^{j} \rangle, \quad (4)$$

where ψ_6^i is the (complex) value of the hexatic bond-orientation order parameter for particle i at position $\mathbf{r}_i$. At low Pe, we observe long-ranged orientational correlations in the crystal and amoeba regimes. Such correlations are significantly shorter ranged for the active gas. Interestingly, for the largest Pe in the banding regime, we find that the bond-orientational order parameter is correlated over a larger domain than in the gas regime. Therefore, formation of the bands not only increases ψ_6, but also enhances its spatial correlations.

D. Dynamical analysis

In our analysis of the local structure in Fig. 2, we noted that some kind of dynamical order parameter would be appropriate to distinguish the crystallites from the amoebae. In Fig. 3, we use such an order parameter to perform this analysis, the overlap [24],

$$Q(t) = \left\langle \frac{1}{N} \sum_{i=1}^{N} \exp - \left(\frac{[\mathbf{r}_i(t' + t) - \mathbf{r}_i(t')]^2}{a^2} \right) \right\rangle_{t'}, \quad (5)$$

which we evaluate at $a = \sigma$. We fit the resulting dynamic correlation functions with a stretched exponential form, where b is the stretching exponent, $Q(t) = \exp[-(t/\tau_\alpha)^b]$, as shown in Fig. 3(a) to determine a timescale for relaxation in our system τ_α. We plot this timescale against the Péclet number in Fig. 3(b).

Most striking in the crystal-amoeba transition is the massive drop in relaxation time [Fig. 3(b)]: At a total of *five* decades, this is a very substantial dynamical change for particle-resolved studies of colloids, active or passive [78]. Thus, the crystallites are effectively solids, while the amoebae exhibit timescales of colloidal liquids, even though their local structure is crystalline. Despite this precipitous drop in relaxation time, we find that the transition from crystallites to amoeba is apparently continuous in nature. We thus conclude that the crystallite-amoebae and amoeba-active gas transitions
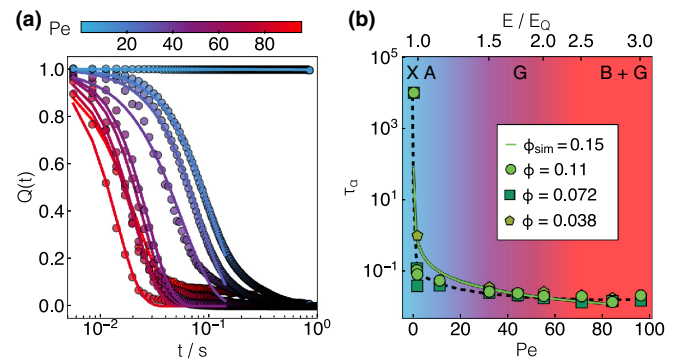

FIG. 3. Dynamics of the Quincke rollers across various phases. (a) Dynamical overlap function $Q(t)$, using Eq. (5). Symbols represent experimental data for $\phi = 0.11$. Solid lines are exponential fits as described in the text, where the stretching exponent b is constrained to 1 for both experiment and simulation. Color bar indicates the correspondent Pe for each line. Data are scaled by the Brownian time τ. (b) Relaxation time τ_α from stretched-exponential fitting to symbols in (a). Symbols represent experiments, solid line is obtained from simulations, and dashed line is a guide. The phases are denoted as X (crystallites), A (amoebae), B + G [(active) gas and banding].
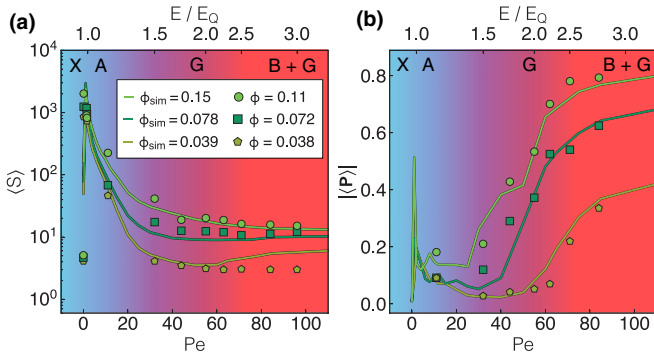
FIG. 4. Characteristics of the clusters formed by the Quincke rollers. (a) Size of clusters as a function of activity. Rapid increase is observed as crystallites form. Symbols represent experiments and lines are from numerical analysis. (b) Polar order for different Pe values. Symbols are data obtained from many velocity measurements over different regions in the sampling cell. As above, the phases are denoted as X (crystallites), A (amoebae), B + G [(active) gas and banding].

we have found are both continuous, at least insofar as we can detect.

E. Characteristics of the active and passive crystallites

In Fig. 2, the ψ_6 bond-orientational order parameter gave somewhat limited insight as to the nature of the crystallite-amoeba transition, as both exhibit hexagonal local symmetry. Therefore, we now seek other structural measures. Figure 4(a) shows how the mean cluster size varies in different regimes. We consider four particles as the minimum cluster size. The system is composed of a few large clusters at very low Pe. Upon increasing the activity, those big clusters break up to smaller ones until in the inhomogeneous regime where the system is dominated by monomers and small clusters from collisions. Hence, the low mean size in Fig. 4(a), despite the emergence of denser bands. Note that in the regime where our simulations indicate banding, finite-size effects in the simulations (which have 10 000 particles) may influence the cluster size somewhat as the bands span the simulation box. The same holds for the passive crystals at low field strength.

F. Nature of the transitions at higher activity: Amoeba to active gas and active gas to ordered bands

In addition to the transitions we have already discussed, we encounter more at higher field strength. First, the amoebae "dissolve" to form an "active gas." At the densities we consider, this transition is characterized by a substantial, but continuous, drop in the ψ_6 bond-orientational order parameter [Fig. 2(a)] consistent with our discussion of the continuous change in dynamics above.

At higher field strengths, we encounter banding, strong density fluctuations perpendicular to the preferred direction of travel. Interestingly, this inhomogeneous state exhibits some degree of local order, as the value of the bond-orientational order parameter $\langle\psi_6\rangle \approx 0.2$. At higher densities, e.g., $\phi \gtrsim 10^{-1}$, the local order of dense bands is notably higher, with

$\langle\psi_6\rangle > 0.5$ [see B+G panel Fig. 1(c)]. While far from indicating full hexagonal order ($\langle\psi_6\rangle = 1$), this is nevertheless significantly larger than zero. Furthermore, as we can see in Fig. 1(c), some particles are in a very high state of crystalline order (appearing blue), although most are not. Previous work did not observe hexagonal ordering [53,54]; we believe this is due to the fact the bands in our case form at much higher area fraction, such that excluded volume effects contribute to the ordering. We note that here we use polymethylmethacrylate particles, while Bricard *et al.* [53,54] used polystyrene particles whose electrostatic charging properties may be different.

Rather striking, in the case of the transition to the banded phase is the alignment between the dipoles of the Quincke rollers, which defines the direction of rotation. In Fig. 4(b), we see a very strong increase in the alignment upon banding, suggesting that this is a suitable order parameter in this case. Taking the polarization $|\langle\mathbf{P}\rangle|$ as an order parameter for the transition between active gas and bands, we find that it is continuous.

IV. DISCUSSION

We have shown that the Quincke roller system exhibits a rich and complex phase behavior, with passive fluid, crystal, amoebalike active crystallites, active gas, and an ordered banding phase. We reveal an intriguing reversal in the roles of active and passive interactions. At low field strength, activity suppresses demixing, while (passive) electrohydrodynamic interactions drive partial demixing in the "amoeba" phase. At high field strength, the situation is quite reversed: Here activity drives partial demixing into bands. This is consistent with recent theoretical predictions for active liquids [41] and the well-known phenomenon of motility-induced phase separation [6].

We have used a variety of static and dynamic order parameters to probe the nature of the transitions between these states, and find that they are continuous in nature except the (passive) fluid-crystal transition which is consistent with first order. One intriguing question concerns the universality of such states in active matter with attractions, and the role of hydrodynamics [79].

For the simulation model, we have quantitatively parametrized the components of the Quincke roller system by treating the electrohydrodynamic attraction with long-ranged potential, "hard"-core, active force, and electrohydrodynamic alignment terms. Remarkably, when we rescale our results to compare the same Péclet numbers in experiments and simulations, we obtain a quantitative agreement between the two. With the model, we have revealed that a key ingredient of the phase behavior is the interplay between *active* and *passive* interactions.

To date, there are few examples of quantitative agreement between particular models and experiments in active matter, and it is in this quantitative agreement between simulation and experiment that our work is significant. Our work opens the way to using simple, intuitive minimal models which correctly capture the *microscopic* interactions to describe, quantitatively, the *macroscopic* physical behavior of complex active systems which are far from equilibrium.

APPENDIX: MATERIALS AND METHODS

1. Experimental setup

Our experimental Quincke roller model consists of poly(methyl methacrylate) (PMMA) spheres of diameter $\sigma = 2.92 \, \mu$m determined with SEM. These are suspended in a 0.15-mM solution of dioctyl sulfosuccinate sodium (AOT) in hexadecane. Imaging and application of a uniform dc field take place in sample cells made of two indium tin oxide (ITO)-coated glass slides (Solems ITOSOL12), separated with a layer of adhesive tape of thickness $H = 100 \, \mu$m. Additionally, a layer of photoresist (Microposit S1818) of $2 \, \mu$m in thickness is deposited on the top electrode. Square confinement regions of 5 mm × 5 mm are created using conventional lithography techniques. The same electric field E that triggers Quincke rotation induces a lateral electric potential gradient between the conductive region and the insulating photoresist layer. As a result, an electrokinetic inward flow confines the rollers at the bottom electrode [61]. The electric field is applied by a power supply (Elektro Automatik, PS-2384-05B) and amplified (Trek 606E-6). Image sequences are obtained using brightfield microscopy (Leica DMI 3000B) with a 10× objective and recorded with a frame rate of 354 fps (Basler Ace). All measurements were performed when the rollers reached a steady state. Individual rollers are identified and particle trajectories are reconstructed using a Python version of conventional tracking methods [80].

2. Determination of the critical strength

We follow the description of Lemaire and coworkers [65,81] to estimate the critical field strength E_Q. The spontaneous rotation of particles, known as Quincke rotation, strongly depends on the charge distribution at the particle-liquid interface and the respective charge relaxation times, given by $\tau_{p,l} = \epsilon_{p,l}/s_{p,l}$, where $\epsilon_{p,l}$ and $s_{p,l}$ are the dielectric constant and conductivity of the particle and the liquid, respectively. In the case of having $\tau_l > \tau_p$, the induced dipole **P** is stable with respect of field direction. On the other hand, with $\tau_p > \tau_l$, **P** is unstable with respect to the field direction [see Fig. 1(a) in main text], and any perturbation results in an electrostatic torque $\mathcal{T}^e = \mathbf{P} \times \mathbf{E}$, from the dipole rotation. Nevertheless, even if $\tau_p > \tau_l$ is satisfied, $\mathcal{T}^e$ needs to overcome the viscous torque exerted on the particle by the liquid to initiate rotation, $\mathcal{T}^H = -\alpha \omega$, where the

angular velocity is given by ω and $\alpha = \pi \eta \sigma^3$ is the rotational friction coefficient. We use polymethyl methacrylate colloids of diameter $\sigma = 2.92 \, \mu$m, with $\epsilon_p = 2.6\epsilon_0$, and a 0.15 mM AOT/hexadecane solution with $\eta = 4.3$ mPa, $s_l \approx 10^{-8}$ S m^{-1} [82], $s_p \approx 10^{-14}$ S m^{-1} [65], and $\epsilon_l \approx 2\epsilon_0$ for our system. The critical threshold is given by

$$E_Q = \left[\tfrac{1}{2} \pi \epsilon_l \sigma^3 (\mathcal{P}^0 - \mathcal{P}^\infty) \tau_{MW} \alpha^{-1} \right]^{-1/2}, \quad \text{(A1)}$$

where the polarizability factors

$$\mathcal{P}^0 = \frac{s_p - s_l}{s_p + 2s_l} \quad \text{(A2)}$$

and

$$\mathcal{P}^\infty = \frac{\epsilon_p - \epsilon_l}{\epsilon_p + 2\epsilon_l} \quad \text{(A3)}$$

account for the conductivities and permittivities of the particle and liquid, respectively. The characteristic dipole relaxation timescale is given by the Maxwell-Wagner time

$$\tau_{MW} = \frac{\epsilon_p + 2\epsilon_l}{s_p + 2s_l}. \quad \text{(A4)}$$

3. Order-parameter details

Here, we take the mean of the bond-orientational order parameter ψ_6 across N particles

$$\psi_6 = \frac{1}{N} \sum_{j=1}^{N} |\psi_6^j|. \quad \text{(A5)}$$

The value of the order parameter for each particle is

$$\psi_6^j \equiv \frac{1}{Z_j} \sum_{k=1}^{Z_j} \exp\left(i6\theta_k^j\right), \quad \text{(A6)}$$

where Z_j is the coordination number of particle j obtained from a Voronoi construction and θ_k^j is the angle made between a reference axis and the bond between particle j and its kth neighbor. $\psi_6 = 1$ indicates perfect hexagonal ordering, whereas completely disordered structures give $\psi_6 = 0$. Figure 2(a) shows that for a passive Brownian system there is almost no hexagonal order. We quantify the fluctuations in ψ_6 by defining the susceptibility

$$\chi_6 \equiv \left\langle \psi_6^2 \right\rangle - \left\langle \psi_6 \right\rangle^2, \quad \text{(A7)}$$

where $\psi_6^2 = 1/N \sum_{j=1}^{N} |\psi_6^j|^2$.

4. Simulation details

Brownian dynamics simulations were performed on a 2D system composed of $N = 10\,000$ interacting Quincke rollers. We integrate the overdamped Langevin equations [Eq. (2)] using the stochastic Euler scheme with a time step of $dt = 10^{-5}\tau$. In our simulations, the interparticle force on the ith roller $\mathbf{F}_i = -\nabla_i(\mathcal{H}_{attr} + \mathcal{H}_{exc})$ while the torque on the ith roller $\mathcal{T}_i = -\partial \mathcal{R}_{align}/\partial \theta_i$. The particle diameter σ, thermal energy $\epsilon = k_B T$, and Brownian time $\tau = \sigma^2/D_t$ are chosen as basic units for length, energy, and time, respectively. We take $D_r = 3D_t/\sigma^2$, as expected for a spherical particle in the low-Reynolds-number regime. We study the phase behavior of

the system as a function of two dimensionless parameters; Péclet number $\text{Pe} = f^p \sigma / k_B T$ and the area fraction $\phi = \frac{N \pi \sigma^2}{4L^2}$, where L is the linear size of the simulation box.

5. Microscopic model of alignment interactions in Quincke rollers

The following description is based on a microscopic model describing the dynamics of a population of colloidal rollers

due to Quincke rotation. The direct interactions are captured in the force $\mathbf{F}_i$ in Eq. (A8). Here we consider the alignment terms. The equations of motion for the ith self-propelled particle are given by the following Langevin equations, where for the rotational case we have rewritten the version in the main text to explicitly consider the effective alignment interaction:

$$\dot{\mathbf{r}}_i = \frac{D_t}{k_B T}[\mathbf{F}_i + f^p \hat{\mathbf{P}}_i] + \sqrt{2D_t}\boldsymbol{\xi}_i^t \tag{A8}$$

and

$$\dot{\theta}_i = -\frac{D_r}{k_B T}\frac{\partial}{\partial \theta_i}\sum_{j \neq i}\mathcal{R}_{\text{align}}(\mathbf{r}_{ij}, \hat{\mathbf{P}}_i, \hat{\mathbf{P}}_j) + \sqrt{2D_r}\xi_i^r, \tag{A9}$$

where the particle i is subject to a propulsion force of magnitude f^p whose direction changes due to the alignment interaction and noise ξ_i. We consider a pairwise alignment interaction between rollers that leads to a torque on particle i. Note that because the simulations are strictly in 2D, the direction of the dipole $\mathbf{P}$ in Eq. (A9) is that of the rotation, i.e., the direction of self-propulsion, rather than the (3D) induced dipole of the experimental system mentioned above.

Introduced by Caussin and Bartolo [53], the effective alignment interaction $\mathcal{R}_{\text{align}}$ reads as

$$\mathcal{R}_{\text{align}}(\mathbf{r}, \hat{\mathbf{P}}_i, \hat{\mathbf{P}}_j) = -A_1(r)\hat{\mathbf{P}}_i \cdot \hat{\mathbf{P}}_j - A_2(r)\hat{\mathbf{r}} \cdot (\hat{\mathbf{P}}_i - \hat{\mathbf{P}}_j) - A_3(r)\hat{\mathbf{P}}_j \cdot (2\hat{\mathbf{r}}\hat{\mathbf{r}} - \mathbf{I}) \cdot \hat{\mathbf{P}}_i, \tag{A10}$$

where $\hat{\mathbf{P}}_i = (\cos\theta_i, \sin\theta_i)$ is the direction of motion of the ith roller, and $\hat{\mathbf{r}} \equiv \mathbf{r}/r$. This has the minimum number of terms required to describe the electrohydrodynamically induced alignment interactions with the correct symmetry and whose range is set by the distance between plates in the experimental setup. We truncate $\mathcal{R}_{\text{align}}$ at $r_{c1} = 3.0\,\sigma$, where σ is the particle diameter. We note that angular momentum is not conserved by these dynamics.

The coefficients $A_1(r)$, $A_2(r)$, and $A_3(r)$ incorporate the microscopic parameters, and are given by

$$A_1(r) = 3\tilde{\mu}_s\frac{\sigma^3}{8r^3}\Theta(r) + 9\left(\frac{\mu_\perp}{\mu_r} - 1\right)\left(\mathcal{P}^\infty + \frac{1}{2}\right)\left(1 - \frac{E_Q^2}{E^2}\right)\frac{\sigma^5}{32r^5}\Theta(r) \tag{A11a}$$

accounting for the short-ranged hydrodynamic interactions and electrostatic couplings that promote the alignment of directions between particles i and j. Here, $\mu_\perp$ and μ_r are the mobility coefficients depending on the liquid viscosity and the distance d between the surface and particle, respectively. From the expressions in [83–86] we obtain $\mathcal{P}^\infty = 0.08$, $\tilde{\mu}_s = 11$, and $\mu_\perp/\mu_r = 1.5$.

The electrostatic repulsion and the electrohydrodynamic interactions coupling are encoded in the $A_2(r)$ and $A_3(r)$ coefficients, respectively,

$$A_2(r) = 6\left(\frac{\mu_\perp}{\mu_r} - 1\right)\sqrt{\frac{E^2}{E_Q^2} - 1}\left[\left(\mathcal{P}^\infty + \frac{1}{2}\right)\frac{E^2}{E_Q^2} - \chi^\infty\right]\frac{\sigma^4}{16r^4}\Theta(r), \tag{A11b}$$

$$A_3(r) = 2\tilde{\mu}_s\frac{\sigma^2}{4r^2}\frac{\sigma}{2H} + \left[\tilde{\mu}_s\frac{\sigma^3}{8r^3} + 5\left(\frac{\mu_\perp}{\mu_r} - 1\right)\left(\mathcal{P}^\infty + \frac{1}{2}\right)\left(1 - \frac{E_Q^2}{E^2}\right)\frac{\sigma^5}{32r^5}\right]\Theta(r), \tag{A11c}$$

where the hydrodynamic and electrostatic couplings are screened over distances proportional to the chamber distance, $H = 100$ μm. A more detailed description can be found in Refs. [53,54]. We estimate such coefficients considering the experimental field intensity under which we observe the active gas phase ($E \geqslant E_Q$, with $E_Q \approx 8 \times 10^5$ V m^{-1}), and average them over distances $r \in [\sigma, 3\sigma]$. For convenience we approximate the screening function as $\Theta(r) = 1$ if $r \leqslant H/\pi$ and $\Theta(r) = 0$ otherwise.

The interparticle force on the ith roller reads as $\mathbf{F}_i = -\nabla_i(\mathcal{H}_{\text{attr}} + \mathcal{H}_{\text{exc}})$, where the electro-osmotic long-ranged attraction [72] is modeled by a truncated and shifted (at $r_{c2} = 5.0\,\sigma$) potential of the form

$$\mathcal{H}_{\text{attr}} = -A_4 \exp(-\kappa r)/r^2, \tag{A12}$$

where $\kappa = 1/3\,\sigma^{-1}$ is the inverse screening length. The excluded volume interactions between rollers are represented by a repulsive Weeks-Chandler-Anderson (WCA) interaction of the form $\mathcal{H}_{\text{exc}} = 4\epsilon[(\sigma/r)^{12} - (\sigma/r)^6] + \epsilon$, where $\epsilon = k_B T$ is the energy unit of the model. The WCA potential is truncated at $r_{c3} = 2^{1/6}\sigma$.

The coupling parameters in the alignment interactions are estimated to be $A_1 = 0.93 k_B T$, $A_2 = 0.33 k_B T$, and $A_3 = 0.48 k_B T$ for our experimental conditions, and we chose the attraction strength to be $A_4 = 10 k_B T$. We verified that the qualitative phase behavior of the model remains the same if we vary the strength of the long-ranged attraction. We note that we have parametrized

A_1, A_3 from the single-particle dynamics in the dilute gas phase, the attractive interactions A_2, A_4 are determined from the experimental parameters.

[1] M. C. Marchetti, J. F. Joanny, S. Ramaswamy, T. B. Liverpool, J. Prost, M. Rao, and R. A. Simha, Hydrodynamics of soft active matter, Rev. Mod. Phys. **85**, 1143 (2013).

[2] M. C. Marchetti, Y. Fily, S. Henkes, A. Patch, and D. Yllanes, Minimal model of active colloids highlights the role of mechanical interactions in controlling the emergent behavior of active matter, Curr. Opin. Colloid Interface Sci. **21**, 34 (2016).

[3] F. Schweitzer, *Brownian Agents and Active Particles* (Springer, Berlin, 2003).

[4] T. Vicsek and A. Zafeiris, Collective motion, Phys. Rep. **517**, 71 (2012).

[5] S. Ramaswamy, The mechanics and statistics of active matter, Annu. Rev. Condens. Matter Phys. **1**, 323 (2010).

[6] M. E. Cates and J. Tailleur, Motility-induced phase separation, Annu. Rev. Condens. Matter Phys. **6**, 219 (2015).

[7] C. Bechinger, R. Di Leonardo, H. Löwen, C. Reichhardt, G. Volpe, and G. Volpe, Active particles in complex and crowded environments, Rev. Mod. Phys. **88**, 045006 (2016).

[8] M. F. Hagan and A. Baskaran, Emergent self-organization in active materials, Curr. Opin. Cell Biol. **38**, 74 (2016).

[9] S. H. L. Klapp, Collective dynamics of dipolar and multipolar colloids: From passive to active systems, Curr. Opin. Coll. Interf. Sci. **21**, 76 (2016).

[10] S. A. Mallory C. Valeriani, and A. Cacciuto, An active approach to colloidal self-assembly, Ann. Rev. Phys. Chem. **69**, 59 (2018).

[11] A. Zöttl and H. Stark, Emergent behavior in active colloids, J. Phys.: Condens. Matter **28**, 253001 (2016).

[12] S. Ramaswamy, Active matter, J. Stat. Mech. (2017) 054002.

[13] G. Ariel, A. Rabani, S. Benisty, J. D. Partridge, R. M. Harshey, and A. Be'er, Swarming bacteria migrate by Lévy Walk, Nat. Commun. **6**, 8396 (2015).

[14] V. Narayan, S. Ramaswamy, and N. Menon, Long-lived giant number fluctuations in a swarming granular nematic, Science **317**, 105 (2007).

[15] I. Theurkauff, C. Cottin-Bizonne, J. Palacci, C. Ybert, and L. Bocquet, Dynamic Clustering in Active Colloidal Suspensions with Chemical Signaling, Phys. Rev. Lett. **108**, 268303 (2012).

[16] J. Palacci, S. Sacanna, A. P. Steinberg, D. J. Pine, and P. M. Chaikin, Living Crystals of Light-Activated Colloidal Surfers, Science **339**, 936 (2013).

[17] E. Mani and H. Löwen, Effect of self-propulsion on equilibrium clustering, Phys. Rev. E **92**, 032301 (2015).

[18] M. N. van der Linden, L. C. Alexander, D. G. A. L. Aarts, and O. Dauchot, Interrupted Motility Induced Phase Separation in Aligning Active Colloids, Phys. Rev. Lett. **123**, 098001 (2019).

[19] T. Speck, J. Bialké, A. M. Menzel, and H. Löwen, Effective Cahn-Hilliard Equation for the Phase Separation of Active Brownian Particles, Phys. Rev. Lett. **112**, 218304 (2014).

[20] I. Buttinoni, J. Bialké, F. Kümmel, H. Löwen, C. Bechinger, and T. Speck, Dynamical Clustering and Phase Separation in Suspensions of Self-Propelled Colloidal Particles, Phys. Rev. Lett. **110**, 238301 (2013).

[21] J. Schwarz-Linek, C. Valeriani, A. Cacciuto, M. E. Cates, D. Marenduzzo, A. N. Morozov, and W. C. K. Poon, Phase separation and rotor self-assembly in active particle suspensions, Proc. Natl. Acad. Sci. USA **109**, 4052 (2012).

[22] J. Barré R. Chétrite, M. Muratori, and F. Peruani, Motility-induced phase separation of active particles in the presence of velocity alignment, J. Stat. Phys. **158**, 589 (2015).

[23] H. Chaté, F. Ginelli, G. Grégoire, and F. Raynaud, Collective motion of self-propelled particles interacting without cohesion, Phys. Rev. E **77**, 046113 (2008).

[24] G. Briand and O. Dauchot, Crystallization of Self-Propelled Hard Discs, Phys. Rev. Lett. **117**, 098004 (2016).

[25] F. Jülicher, K. Kruse, J. Prost, and J.-F. Joanny, Active behavior of the cytoskeleton, Phys. Rep. **449**, 3 (2007).

[26] T. Sanchez, D. T. Chen, S. J. DeCamp, M. Heymann, and Z. Dogic, Spontaneous motion in hierarchically assembled active matter, Nature (London) **491**, 431 (2012).

[27] J.-A. Park, J. H. Kim, D. Bi, J. A. Mitchel, N. T. Qazvini, K. Tantisira, C. Y. Park, M. McGill, S.-H. Kim, B. Gweon, J. Notbohm, R. Steward, Jr., S. Burger, S. H. Randell, A. T. Kho, D. T. Tambe, C. Hardin, S. A. Shore, E. Israel, D. A. Weitz *et al.*, Unjamming and cell shape in the asthmatic airway epithelium, Nat. Mater. **14**, 1040 (2015).

[28] T. Pedley and J. Kessler, Hydrodynamic phenomena in suspensions of swimming microorganisms, Annu. Rev. Fluid Mech. **24**, 313 (1992).

[29] H. P. Zhang, A. Be'er, E.-L. Florin, and H. L. Swinney, Collective motion and density fluctuations in bacterial colonies, Proc. Natl. Acad. Sci. USA **107**, 13626 (2010).

[30] E. Lushi, H. Woiland, and R. E. Goldstein, Fluid flows created by swimming bacteria drive self-organization in confined suspensions, Proc. Natl. Acad. Sci. USA **111**, 9733 (2014).

[31] A. P. Petroff, X. L. Wu, and A. Libchaber, Fast-Moving Bacteria Self-Organize into Active Two-Dimensional Crystals of Rotating Cells, Phys. Rev. Lett. **114**, 158102 (2015).

[32] M. Sinhuber and N. T. Ouellette, Phase Coexistence in Insect Swarms, Phys. Rev. Lett. **119**, 178003 (2017).

[33] Y. Katz, K. Tunstrom, C. C. Ioannou, C. Huepe, and I. D. Couzin, Inferring the structure and dynamics of interactions in schooling fish, Proc. Natl. Acad. Sci. USA **108**, 18720 (2011).

[34] A. Cavagna, A. Cimarelli, I. Giardina, G. Parisi, R. Santagati, F. Stefanini, and M. Viale, Scale-free correlations in starling flocks, Proc. Natl. Acad. Sci. USA **107**, 11865 (2010).

[35] G. Volpe, I. Buttinoni, D. Vogt, H.-J. Kümmerer, and C. Bechinger, Microswimmers in patterned environments, Soft Matter **7**, 8810 (2011).

[36] G. Vizsnyiczai, G. Frangipane, C. Maggi, F. Saglimbeni, S. Bianchi, and R. Di Leonardo, Light controlled 3d micromotors powered by bacteria, Nat. Commun. **8**, 15974 (2017).

[37] D. Mandal, K. Klymko, and M. R. DeWeese, Entropy Production and Fluctuation Theorems for Active Matter, Phys. Rev. Lett. **119**, 258001 (2017).

[38] A. Souslov, B. C. van Zuiden, D. Bartolo, and V. Vitelli, Topological sound in active-liquid metamaterials, Nat. Phys. **13**, 1091 (2017).

[39] M. Han, J. Yan, S. Granick, and E. Luijten, Effective temperature concept evaluated in an active colloid mixture, Proc. Natl. Acad. Sci. USA **114**, 7513 (2017).

[40] S. Paliwal, J. Rodenburg, R. van Roij, and M. Dijkstra, Chemical potential in active systems: Predicting phase equilibrium from bulk equations of state? New J. Phys. **20**, 015003 (2018).

[41] E. Tjhung, C. Nardini, and M. E. Cates, Cluster Phases and Bubbly Phase Separation in Active Fluids: Reversal of the Ostwald Process, Phys. Rev. X **8**, 031080 (2018).

[42] C. Nardini, É. Fodor, E. Tjhung, F. van Wijland, J. Tailleur, and M. E. Cates, Entropy Production in Field Theories without Time-Reversal Symmetry: Quantifying the Non-Equilibrium Character of Active Matter, Phys. Rev. X **7**, 021007 (2017).

[43] L. Dabelow, S. Bo, and R. Eichhorn, Irreversibility in Active Matter Systems: Fluctuation Theorem and Mutual Information, Phys. Rev. X **9**, 021009 (2019).

[44] T. Vicsek, A. Czirók, E. Ben-Jacob, I. Cohen, and O. Shochet, Novel Type of Phase Transition in a System of Self-Driven Particles, Phys. Rev. Lett. **75**, 1226 (1995).

[45] G. Grégoire and H. Chaté, Onset of Collective and Cohesive Motion, Phys. Rev. Lett. **92**, 025702 (2004).

[46] S. Wang and P. G. Wolynes, On the spontaneous collective motion of active matter, Proc. Natl. Acad. Sci. USA **108**, 15184 (2011).

[47] B. M. Mognetti, A. Saric, S. Angioletti-Uberti, A. Cacciuto, C. Valeriani, and D. Frenkel, Living Clusters and Crystals from Low-Density Suspensions of Active Colloids, Phys. Rev. Lett. **111**, 245702 (2013).

[48] G. S. Redner, M. F. Hagan, and A. Baskaran, Structure and Dynamics of a Phase-Separating Active Colloidal Fluid, Phys. Rev. Lett. **110**, 055701 (2013).

[49] J. Stenhammar, A. Tiribocchi, R. J. Allen, D. Marenduzzo, and M. E. Cates, Continuum Theory of Phase Separation Kinetics for Active Brownian Particles, Phys. Rev. Lett. **111**, 145702 (2013).

[50] É. Fodor, C. Nardini, M. E. Cates, J. Tailleur, P. Visco, and F. van Wijland, How Far from Equilibrium Is Active Matter? Phys. Rev. Lett. **117**, 038103 (2016).

[51] O. Pohl and H. Stark, Dynamic Clustering and Chemotactic Collapse of Self-Phoretic Active Particlesoliver Pohl1and Holger Stark, Phys. Rev. Lett. **112**, 238303 (2014).

[52] A. Zöttl and H. Stark, Hydrodynamics Determines Collective Motion and Phase Behavior of Active Colloids in Quasi-Two-Dimensional Confinement, Phys. Rev. Lett. **112**, 118101 (2014).

[53] A. Bricard, J.-B. Caussin, N. Desreumaux, O. Dauchot, and D. Bartolo, Emergence of macroscopic directed motion in populations of motile colloids, Nature (London) **503**, 95 (2013).

[54] A. Bricard, J.-B. Caussin, D. Das, C. Savoie, V. Chikkadi, K. Shitara, O. Chepizhko, F. Peruani, D. Saintillan, and D. Bartolo, Emergent vortices in populations of colloidal rollers, Nat. Commun. **6**, 7470 (2015).

[55] D. Geyer, D. Martin, J. Tailleur, and D. Bartolo, Freezing a Flock: Motility-Induced Phase Separation in Polar Active Liquids, Phys. Rev. X **9**, 031043 (2019).

[56] D. Andelman and M. Seul, Domain shapes and patterns: The phenomenology of modulated phases, Science **267**, 476 (1995).

[57] F. Sciortino, S. Mossa, E. Zaccarelli, and P. Tartaglia, Equilibrium Cluster Phases and Low-Density Arrested Disordered States: The Role of Short- Range Attraction and Long-Range Repulsion, Phys. Rev. Lett. **93**, 055701 (2004).

[58] A. J. Archer and N. B. Wilding, Phase behavior of a fluid with competing attractive and repulsive interactions, Phys. Rev. E **76**, 031501 (2007).

[59] A. Ciach, Universal sequence of ordered structures obtained from mesoscopic description of self-assembly, Phys. Rev. E **78**, 061505 (2008).

[60] A. Jákli, B. Senyuk, G. Liao, and O. D. Lavrentovich, Colloidal micromotor in smectic A liquid crystal driven by DC electric field, Soft Matter **4**, 2471 (2008).

[61] S.-R. Yeh, M. Seul, and B. I. Shraiman, Assembly of ordered colloidal aggregates by electric-field-induced fluid flow, Nature (London) **386**, 57 (1997).

[62] W. D. Ristenpart, I. A. Aksay, and D. A. Saville, Assembly of colloidal aggregates by electrohydrodynamic flow: Kinetic experiments and scaling analysis, Phys. Rev. E **69**, 021405 (2004).

[63] K.-Q. Zhang and X. Y. Liu, In situ observation of colloidal monolayer nucleation driven by an alternating electric field, Nature (London) **429**, 739 (2004).

[64] G. Quincke, Ueber Rotationen im constanten electrischen Felde, Ann. Phys. Chemie **295**, 417 (1896).

[65] N. Pannacci, L. Lobry, and E. Lemaire, How Insulating Particles Increase the Conductivity of a Suspension, Phys. Rev. Lett. **99**, 094503 (2007).

[66] D. Das and D. Saintillan, Electrohydrodynamic interaction of spherical particles under Quincke rotation, Phys. Rev. E **87**, 043014 (2013).

[67] See Supplemental Material at http://link.aps.org/supplemental/10.1103/PhysRevE.102.032609 for more details of the mapping of field strength to Péclet number, and for information of Supplemental Movies.

[68] J. Toner and Y. Tu, Long-Range Order in a Two-Dimensional Dynamical xy Model: How Birds Fly Together, Phys. Rev. Lett. **75**, 4326 (1995).

[69] C. A. Weber, T. Hanke, J. Deseigne, S. Léonard, O. Dauchot, E. Frey, and H. Chaté, Long-Range Ordering of Vibrated Polar Disks, Phys. Rev. Lett. **110**, 208001 (2013).

[70] J. B. Caussin, A. Solon, A. Peshkov, H. Chate, T. Dauxois, J. Tailleur, V. Vitelli, and D. Bartolo, Emergent Spatial Structures in Flocking Models: A Dynamical System Insight, Phys. Rev. Lett. **112**, 148102 (2014).

[71] V. Schaller, C. Weber, C. Semmrich, E. Frey, and A. R. Bausch, Polar patterns of driven filaments, Nature (London) **467**, 73 (2010).

[72] F. Nadal, F. Argoul, P. Kestener, B. Pouligny, C. Ybert, and A. Ajdari, Electrically induced flows in the vicinity of a dielectric stripe on a conducting plane, Eur. Phys. J. E **9**, 387 (2002).

[73] H. Karani, G. E. Pradillo, and P. M. Vlahovska, Tuning the Random Walk of Active Colloids: From Individual Run-and-Tumble to Dynamic Clustering, Phys. Rev. Lett. **123**, 208002 (2019).

[74] Z. Shen, A. Würger, J. S. Lintuvuori, Hydrodynamic self-assembly of active colloids: Chiral spinners and dynamic crystals, Soft Matter **15**, 1508 (2019).

[75] C. P. Royall, Hunting mermaids in real space: Known knowns, known unknowns and unknown unknowns, Soft Matter, **14**, 4020 (2018).

[76] A. P. Solon, H. Chaté, and J. Tailleur, From Phase to Microphase Separation in Flocking Models: The Essential Role of Nonequilibrium Fluctuations, Phys. Rev. Lett. **114**, 068101 (2015).

[77] E. P. Bernard and W. Krauth, Two-Step Melting in Two Dimensions: First-Order Liquid-Hexatic Transition, Phys. Rev. Lett. **107**, 155704 (2011).

[78] A. Ivlev, H. Löwen, G. E. Morfill, and C. P. Royall, *Complex Plasmas and Colloidal Dispersions: Particle-resolved Studies of Classical Liquids and Solids* (World Scientific, Singapore, 2012).

[79] F. Alarcón, C. Valeriani, and I. Pagonabarra, Morphology of clusters of attractive dry and wet self-propelled spherical particle suspensions, Soft Matter **13**, 814 (2017).

[80] J. Crocker and D. Grier, Methods of digital video microscopy for colloidal studies, J. Colloid Interface Sci. **179**, 298 (1996).

[81] N. Pannacci, E. Lemaire, and L. Lobry, DC conductivity of a suspension of insulating particles with internal rotation, Eur. Phys. J. E **28**, 411 (2009).

[82] J. Schmidt, R. Prignitz, D. Peschka, A. Münch, B. Wagner, E. Bänsch, and W. Peukert, Conductivity in nonpolar media: Experimental and numerical studies on sodium AOT–hexadecane, lecithin–hexadecane and aluminum(III)-3,5-diisopropyl salicylate–hexadecane systems, J. Colloid. Interface Sci. **386**, 240 (2012).

[83] M. E. O'Neill and K. Stewartson, On the slow motion of a sphere parallel to a nearby plane wall, J. Fluid Mech. **27**, 705 (1967).

[84] A. J. Goldman, R. G. Cox, and H. Brenner, Slow viscous motion of a sphere parallel to a plane wall—II Couette flow, Chem. Eng. Sci. **22**, 653 (1967).

[85] A. J. Goldman, R. G. Cox, and H. Brenner, Slow viscous motion of a sphere parallel to a plane wall—I Motion through a quiescent fluid, Chem. Eng. Sci. **22**, 637 (1967).

[86] Q. Liu and A. Prosperetti, Wall effects on a rotating sphere, J. Fluid Mech. **657**, 1 (2010).